On Cavity Flow Simulating Vortex Induced in the Low Q Low V Layer

Osamu KINOSHITA*, Hidetoshi SHIBUYA* and Hidebumi ITÔ*

(Received June 16, 1986)

Two types of cavity flow are investigated experimentally and computationally as models simulating vortex which would be induced in the low Q low V layer by a subsiding oceanic plate in a trench-arc system. In Model I, the cavity is bounded by semi-infinite parallel walls and a cavity mouth intersects them obliquely with angle θ. In Model II, the wedge-shaped corner of the cavity is partly replaced by solid. As a result, the position of vortex center and the total flow quantity of vortex in Model II scarecely vary from those in Model I, until the maximum thickness of the solid part becomes a value which is about three eighths of the thickness of the fluid layer for small angles as θ = 30° and 45° or a quarter for large angles as 60° and 75°.

1. Introduction

In a trench-arc system, it has been considered that vortex is induced in the low Q low V layer by a subsiding oceanic plate[1,2]. This can be modeled as the two-dimensional cavity flow having the shape as shown in Fig. 1, where the operating fluid is contained in AB′DE, parallel walls AB′ and DE are fixed and B′D is a moving wall with a constant speed. The flow is steady and has a characteristic of very low Reynolds number. Investigation of this cavity flow has shown a result that shear stress along the moving wall is very large near the point B′[2]. Therefore the downgoing slab would not induced any flow near the wedge corner of B′ to slip against mantle. Thus it is desirable that the wedge-shaped corner BB′C is replaced by solid, where BC may correspond to the aseismic front. In this paper, the former AB′DE and the latter ABCDE are called Model I and Model II respectively, and the both vortexes are compared. The investigations are done by experiments for various dip angle θ and by computational simulations for θ = 45°. Kinoshita and Itô have taken charge of the experiments and Shibuya

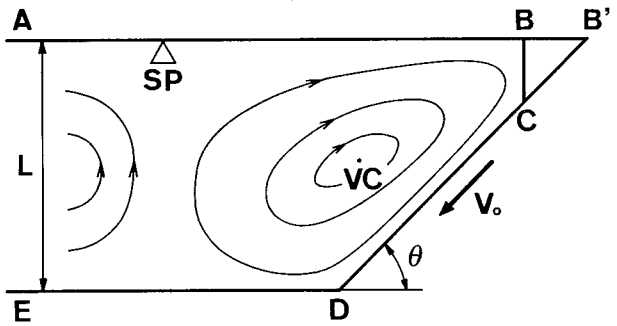

Fig. 1 Illustrative diagram of cavity models. Model I: AB′DE, Model II: ABCDE, SP: stagnation point, VC: vortex center.

* College of Integrated Arts and Sciences.

has done charge of the computational simulations.

2. Analyses by Experiments

The experimental method has been mentioned in Itô et al.[2] and Kinoshita and Itô[3]. The photographs of flow patterns for Model I have been also shown for dip angles $\theta = 90°, 75°, 60°, 45°$ and $30°$[2]. In this paper, for each of these dip angles, BC is taken to be a quarter of the thickness L of the fluid layer and moreover for $\theta = 30°$, BC $= 3L/8$ and $L/2$ are added. In Fig. 2 the flow patterns obtained for Model II are shown. An actual size of the thickness L is 4 cm for all photographs. These photographs are taken by means of switching on and off the light with switching interval 5 seconds. The illuminated paths are trajectories of minute air bubbles mixed in the operating fluid (water glass). In order to obtain the velocity distribution of flow as well as the flow pattern, four switching intervals of 5, 10, 20 and 30 seconds have been used, because lengths of the trajectories depend largely on the position of flow. Each of the photographs for Model I shown in the previous paper[2] was taken in 2 minute exposure to obtain only the flow pattern. In that case, as very minute bubbles were used, delicate streamlines were photographed. To obtain the velocity distribution, however, slightly larger bubbles are suitable as seen in Fig. 2.

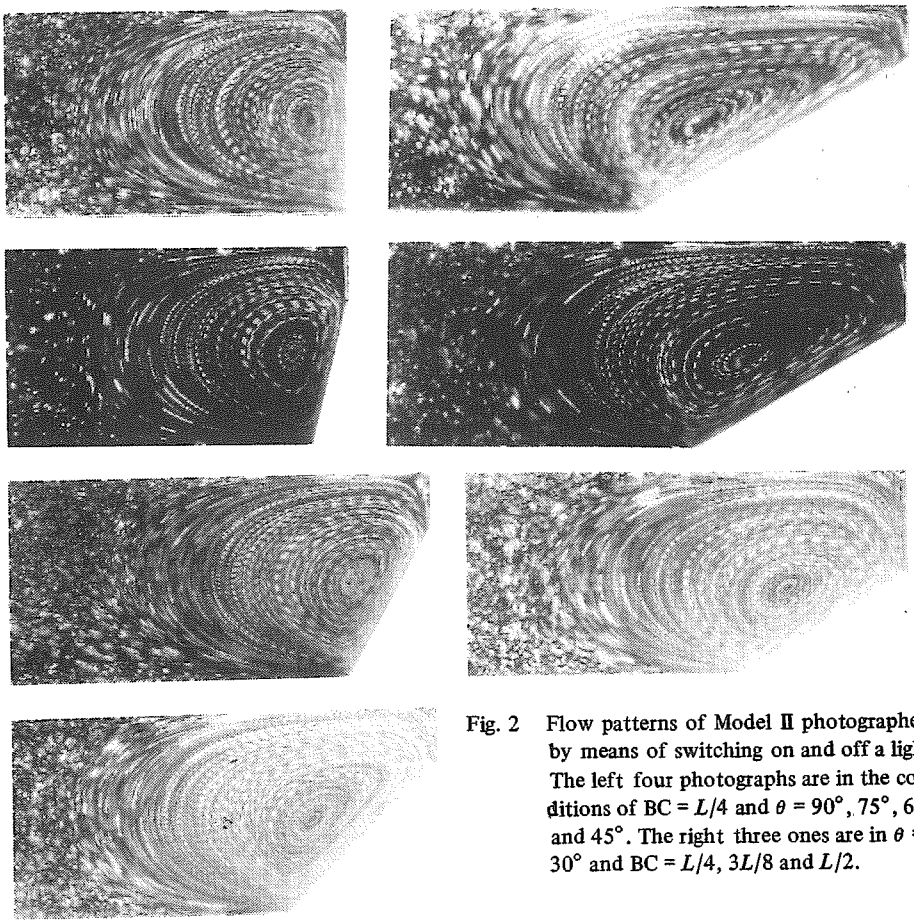

Fig. 2 Flow patterns of Model II photographed by means of switching on and off a light. The left four photographs are in the conditions of BC = $L/4$ and $\theta = 90°, 75°, 60°$ and $45°$. The right three ones are in $\theta = 30°$ and BC = $L/4$, $3L/8$ and $L/2$.

In these photographs the first vortex is seen sharply, but the second vortex is not well observed, which is induced by the first vortex. Hence, only the first vortex is taken up in the experiment.

Figure 3 shows the positions of the vortex center for various dip angles θ in Models I and II, where the vertical and horizontal scales are normalized by L and each of the inclined lines shows the moving wall. The positions of the vortex center in Model II with BC = $L/4$ are considered to be almost the same with those in the Model I excepting $\theta = 90°$. There is a tendency that, when the dip angle of moving wall decreases, the vortex center moves away gradually from the moving wall. When $\theta = 90°$, the vortex center for BC = $L/4$ shifts distinctly from that in Model I. When $\theta = 30°$, the vortex center does not shift till BC becomes $3L/8$, but the vortex center for BC = $L/2$ shifts distinctly.

Figure 4 shows the relationship between the dip angle θ and the position of stagnation point, where s is the distance from the wedge corner B′ to the stagnation point

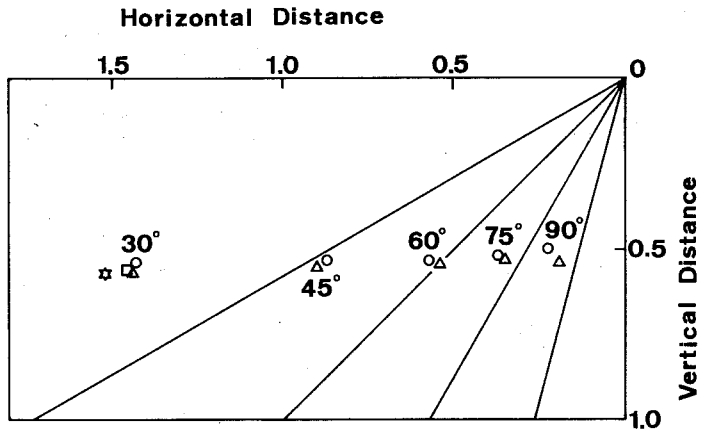

Fig. 3 Positions of the vortex center obtained by experiments for Models I and II. Each of inclined lines shows the moving wall. Vertical and horizontal scales are normalized by the thickness L of fluid layer. Circle; BC = 0, triangle; BC = $L/4$, square; BC = $3L/8$, star; BC = $L/2$.

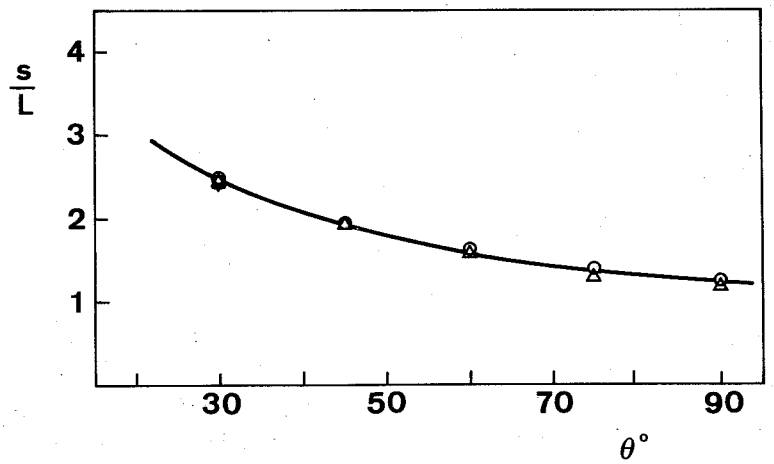

Fig. 4 Relation between dip angle θ and position of the stagnation point. The length s is measured from the wedge corner B′. The symbols are the same as Fig. 3.

dividing the first vortex and the second one (ref. Fig. 1). As seen in Fig. 2, it is ambiguous to settle the stagnation point from only one photograph. The settlement has been done by comparing many photographs with different switching intervals. The stagnation points of Model II examined here are almost unchanged from ones of Model I. This figure is useful to know an extent of the first vortex.

Figure 5 is a comparison between streamlines of Model I and those of Model II for $\theta = 30°$, where each streamline is affixed by a value of the normalized stream function. Figures 5(a) and (b) have been already obtained by Kinoshita and Itô[3] and Kinoshita et al.[4] respectively. A boundary (AB′DE in Model I or ABCDE in Model II) is one streamline. The stream function ψ' is a volume of flow between the streamline and the boundary, provided $\psi' = 0$ at the boundary. The values of stream function in Fig. 5 were calculated by this way from velocity distribution (ref. Fig. 2). The normalized one ψ is given by

$$\psi = \psi'/V_0 L ,$$

where V_0 is velocity of the moving wall. Values of the stream function at the vortex center in Figs. 5(a) and (b) are 0.123 and 0.124 respectively, being nearly equal. However, it is noteworthy that the former is a little less than the latter as will be mentioned later.

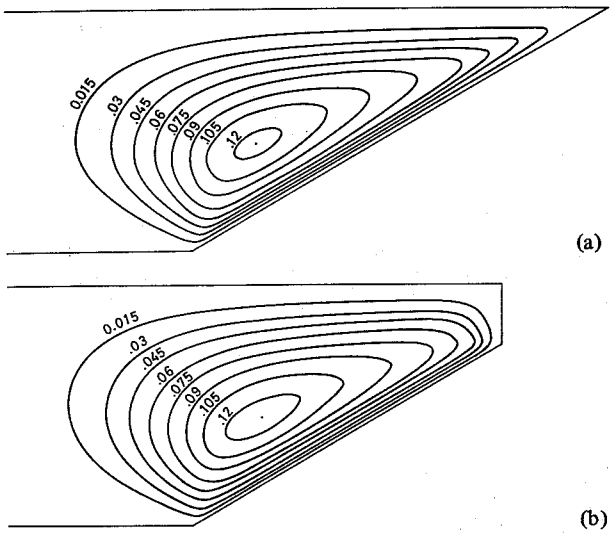

Fig. 5 Streamlines with values of stream function for $\theta = 30°$.

The stream function at the vortex center is a total volume of flow of the first vortex. These values for $\theta = 30°$, 60° and 90° in Model I have been obtained to be 0.123, 0.109 and 0.105 respectively[3]. The values for $\theta = 45°$ and 75° in Model I may be estimated by an interpolation to be 0.114 and 0.106 respectively. Since the total volume of flow equals that between the vortex center and the moving wall, it must be concerned closely with the position of vortex center. The relation between the total volume of flow and the dip angle in Model I is consistent with the tendency in Fig. 3 that the vortex center is far off from the moving wall with decreasing dip angle. On the

other hand, if the positions in Models I and II are the same, their total volumes of flow are also the same. When $\theta = 30°$, the volume of flow is considered to be nearly constant till BC becomes $3L/8$. Also the total volume of flow in Model II with BC $= L/4$ for each of $\theta = 45°$, $60°$ and $75°$ is estimated to be the same as that in Model I. When $\theta = 90°$, the total volume of flow with BC $= L/4$ must be smaller than that with BC $= 0$, because the former vortex center is nearer to the moving wall than the latter one.

3. Analyses by Computational Simulation

In order to confirm the experimental results, a series of computational simulation analyses for $\theta = 45°$ with various ratio of BC/L and for $\theta = 90°$ was performed.

The models calculated are two-dimensional. Since the Reynolds number of the flow concerned is extremely small, the governing equation for the two-dimensional flow is

$$\nabla^4 \psi = 0$$

where ψ is stream function related with velocity components (u, v) by the following equations.

$$u = -\frac{\partial \psi}{\partial y}$$

$$v = \frac{\partial \psi}{\partial x}$$

The boundary conditions assumed in the series of $\theta = 45°$ are as follows: Firstly, the stream function equals zero on all the boundaries, secondly, the velocity is zero at the top (AB in Fig. 1), the bottom (DE) and the vertical portion of right end (BC) of the cavity, thirdly, at the left end of the cavity (AE), the horizontal component of velocity is zero, and lastly the diagonal portion of the right end (CD) moves at unit velocity, where the thickness of the cavity (L) is taken as the unit length. For $\theta = 90°$, the whole right vertical boundary moves at unit velocity, while other boundary conditions are the same as for $\theta = 45°$.

To solve this problem, we employed finite differential method. The dimension of the mesh used for the calculation was 33 X 97, and the triangular portion out of the diagonal moving boundary for the series of $\theta = 45°$ was filled with zero. In a case of $\theta = 45°$ and BC = 0 calculations with reduced meshes of 5 X 13, 9 X 25 and 17 X 49 were made in order to assess the error due to finite mesh, and the difference of maximum value of the stream function between the finest mesh and the second finest mesh was found to be less than 1%. The matrix was solved using ILUCR (Incomplete LU decomposition and Conjugate Residual) method[5], because of its significant advantage both on storage consumption and speed. A FORTRAN program for ILUCR was coded by Shibuya, one of the authors, modifying the program presented in Murata et al.[5]. The machine used is NEC ACOS-850/8 system situated in Computer Center, University of Osaka Prefecture.

The results are illustrated in Figs.6 and 7. Figure 6 shows visually how pattern of the

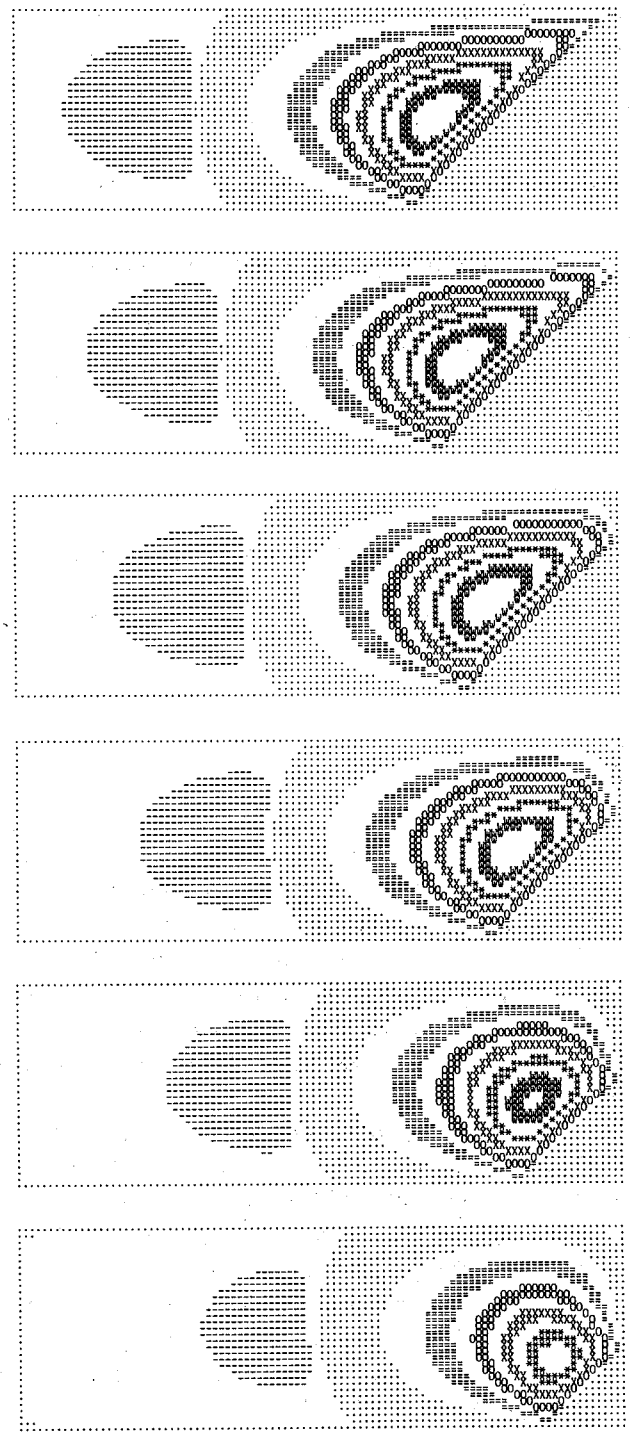

Fig. 6 Flow patterns obtained by computational simulations for $\theta = 45°$ and BC/L = 0, 1/8, 1/4, 3/8, 1/2 and 5/8. Symbols show the following values of stream function respectively; −: −0.001 to −0.0001, ·: 0 to 0.001, =: 0.01 to 0.02, O: 0.03 to 0.04, X: 0.05 to 0.06, ∗: 0.07 to 0.08 and W: 0.09 to 0.10.

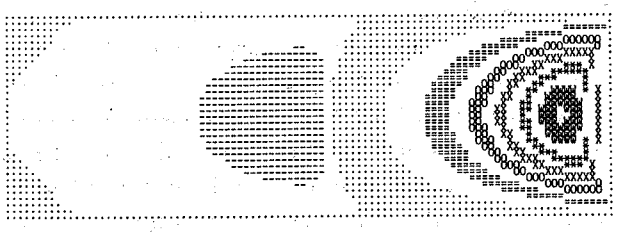

Fig. 7 Flow pattern for $\theta = 90°$ in Model I. Symbols are the same as Fig. 6. Positions of vortex center and total flow quantities are (0.23, 0.5) and 0.101 for the first vortex and (1.63, 0.5) and 0.302×10^{-3} for the second vortex, and position of stagnation point is (1.25, 0).

first vortex changes with the ratio BC/L. The change may be represented by the position of vortex center, the total volume of flow and the position of stagnation point. They are summarized in Table 1, where the positions are measured from the wedge corner B′. This computational analysis has revealed the second vortex which is very weak compared with the first one. The position of center and the total volume of flow for this vortex are also shown in Table 1. The total volume of flow is 3×10^{-3} times of that of the first one. As to Fig. 7, the position of vortex center and the total volume of flow for each of the first and the second vortexes are described in the figure caption.

The positions of vortex center and stagnation point obtained by computational techniques well coincide with those by the experiments (Figs. 3 and 4) for each of the three cases of ($\theta = 90°$, BC = 0), (45°, 0) and (45°, L/4). The total volume of flow is also coinside with each other, although the computational technique is always somewhat smaller than that by the experiment for each case, that is, 0.101 vs. 0.105 for (90°, 0); 0.108 vs. 0.114 for (45°, 0); 0.109 vs. 0.114 for (45°, L/4).

Table 1 Positions of vortex center (VC) and total flow quantities for the first and second vortexes and position of stagnation point (SP), for $\theta = 45°$ and various BC/L obtained by computational simulations.

BC/L	The First Vortex			Position of SP	The Second Vortex		
	Position of VC		Total Flow Quantity		Position of VC		Total Flow Quantity
	Horizontal Distance	Vertical Distance			Horizontal Distance	Vertical Distance	
0	0.91	0.54	0.108	1.94	2.31	0.5	0.327×10^{-3}
1/8	0.90	0.54	0.109	1.94	2.31	0.5	0.327×10^{-3}
1/4	0.90	0.54	0.109	1.94	2.31	0.5	0.327×10^{-3}
3/8	0.90	0.55	0.108	1.95	2.31	0.5	0.323×10^{-3}
1/2	0.93	0.59	0.102	1.96	2.34	0.5	0.295×10^{-3}
5/8	0.96	0.66	0.085	1.99	2.38	0.5	0.223×10^{-3}

4. Conclusion

It has been considered on Model II that, if the moving wall CD draging the fluid is short, the total volume of flow is small and the vortex center nears the moving wall. Also the total volume of flow and the vortex center in Model II has been expected to be smaller and nearer to the moving wall than those in Model I. However, Table 1 for $\theta = 45°$ shows that the position of vortex center and the total volume of flow are almost unchanged till BC becomes 3L/8 and the above expectation appears when BC exceeds

$L/2$. Figure 3 shows that the position of vortex center in Model II with BC $= L/4$ is almost unchanged from that in Model I, excepting $\theta = 90°$. The total volume of flow in Model II with BC $= L/4$ may be also nearly equal to that in Model I excepting $\theta = 90°$, although this has been confirmed for $\theta = 30°$ and 45° (Figs. 5 and 6). When dip angle θ tends to 90°, a difference between Model I and Model II, as for the vortex center and the volume of flow, may be severely subject to an influence of length BC. For smaller dip angle such as 45° or 30° the difference does not appear, till BC becomes about $3L/8$.

As seen in Fig. 5 and Table 1, there is a tendency that Model II with small BC/L has a little larger volume of flow than Model I. Though the difference between their volumes of flow may be not significant, the tendency is contrary to the above expectation to be noticed.

References

1) D.P. McKenzie, Geophys. J. Roy. Astron. Soc., **18**, 1 (1969).
2) H. Itô, Y. Masuda and O. Kinoshita, Bull. Univ. Osaka Pref., **A32**, 47 (1983).
3) O. Kinoshita and H. Itô, J. Fluid Control, **15**, 65 (1984).
4) O. Kinoshita, H. Itô and Y. Masuda, Bull. Univ. Osaka Pref., **A32**, 65 (1983).
5) K. Murata, T. Oguni and Y. Karaki, "Super Computer, –Its application to Scientific Calculation–", p. 304, Maruzen, Tokyo. (in Japanese) (1985).